Naval Research Laboratory

Washington, DC 20375-5320

NRL/MR/6750--00-8449

The Effect of Electric Field Structure on Joule Heating

D.N. WALKER
W.E. AMATUCCI

Charged Particle Physics Branch
Plasma Physics Division

G. GANGULI

Beam Physics Branch
Plasma Physics Division

May 31, 2000

REPORT DOCUMENTATION PAGE

Form Approved
OMB No. 0704-0188

1. AGENCY USE ONLY (*Leave Blank*)	2. REPORT DATE	3. REPORT TYPE AND DATES COVERED
	May 31, 2000	Interim

4. TITLE AND SUBTITLE

The Effect of Electric Field Structure on Joule Heating

5. FUNDING NUMBERS

6. AUTHOR(S)

D.N. Walker, W.E. Amatucci, and G. Ganguli

7. PERFORMING ORGANIZATION NAME(S) AND ADDRESS(ES)

Naval Research Laboratory
Washington, DC 20375-5320

8. PERFORMING ORGANIZATION REPORT NUMBER

NRL/MR/6750--00-8449

9. SPONSORING/MONITORING AGENCY NAME(S) AND ADDRESS(ES)

Office of Naval Research
800 N. Quincy Street
Arlington, VA 22217

10. SPONSORING/MONITORING AGENCY REPORT NUMBER

11. SUPPLEMENTARY NOTES

12a. DISTRIBUTION/AVAILABILITY STATEMENT

Approved for public release; distribution unlimited.

12b. DISTRIBUTION CODE

13. ABSTRACT (*Maximum 200 words*)

We have recently performed a detailed characterization of ion Joule heating perpendicular to an axial magnetic field in the laboratory in a simulated ionospheric plasma environment which contains localized electric field structuring. Since Joule heating is often regarded as an important mechanism contributing to energization of outflowing heavy ions observed by higher altitude auroral satellites, this work has particular relevance to space physics issues; and, to our knowledge, has not been investigated systematically in a controlled environment. Since transverse (to B) ionospheric electric fields are rarely uniform but tend to show spatial and temporal structure, often as small as an ion gyroradius, the ability to systematically vary the spatial extent and magnitude of the electric field region and to observe the effect on ion energy is important. The experiment makes use of a concentric set of separately biasable ring anodes which generate a radial electric field with controllable scale length perpendicular to an ambient axial magnetic field. Joule heating results from ion-neutral collisions occurring within this transverse, dc electric field region.

14. SUBJECT TERMS

15. NUMBER OF PAGES
19

16. PRICE CODE

17. SECURITY CLASSIFICATION OF REPORT	18. SECURITY CLASSIFICATION OF THIS PAGE	19. SECURITY CLASSIFICATION OF ABSTRACT	20. LIMITATION OF ABSTRACT
UNCLASSIFIED	UNCLASSIFIED	UNCLASSIFIED	UL

NSN 7540-01-280-5500

Standard Form 298 (Rev. 2-89)
Prescribed by ANSI Std 239-18
298-102

TABLE OF CONTENTS

Section		Page
ABSTRACT		1
I	**Introduction**	1
II	**Experimental Environment and Measurement Description**	3
III	**Electric Field Shaping and Localization**	4
	An example of varying localization with electric field constant	4
IV	**Results and Conclusions**	5
	Equilibrium properties of the plasma	5
	Comparison to Joule heating rate	5
V	**Acknowledgments**	7
VI	**References**	8

The effect of electric field structure on Joule heating

D.N. Walker[1], W.E. Amatucci[1], and G. Ganguli[2]

[1]Charged Particle Physics Branch
[2]Beam Physics Branch
Plasma Physics Division
Naval Research Laboratory
Washington, DC

Abstract

We have recently performed a detailed characterization of ion Joule heating perpendicular to an axial magnetic field in the laboratory in a simulated ionospheric plasma environment which contains localized electric field structuring. Since Joule heating is often regarded as an important mechanism contributing to energization of outflowing heavy ions observed by higher altitude auroral satellites, this work has particular relevance to space physics issues; and, to our knowledge, has not been investigated systematically in a controlled environment. Since transverse (to B) ionospheric electric fields are rarely uniform but tend to show spatial and temporal structure, often as small as an ion gyroradius, the ability to systematically vary the spatial extent and magnitude of an electric field region and to observe the effect on ion energy, is important. The experiment makes use of a concentric set of separately biasable ring anodes which generate a radial electric field with controllable scale length perpendicular to an ambient axial magnetic field. Joule heating results from ion-neutral collisions occurring within this transverse, dc electric field. Until there is sufficient neutral pressure to raise the ion-neutral collision frequency(ν_{in}) to an observable Joule heating threshold, ion cyclotron wave heating, which is induced by shear in **E×B** rotation, can be the primary channel for ion energization. We have discussed in earlier papers the conditions under which this occurs and treated the transition between the two forms of ion heating. We concentrate primarily in this work on constructing the fields themselves and on the relationship between the subsequent collisional heating and the Pedersen conductivity as an initial indication of the validity of the measurement results

I. Introduction

Joule heating in the ionosphere can be induced by transverse electric fields in a collisional plasma. Collisions between ions and neutrals are integral to the Joule heating process since they

Manuscript approved May 3, 2000.

lead to a cross-magnetic field (Pedersen) current density, $\mathbf{J}_P$, and therefore a $\mathbf{J}_P \cdot \mathbf{E}$ dissipation of electric field energy. Classically, Joule heating assumes a uniform electric field but often ionospheric electric fields are structured. The outstanding question is: How will the structure in the field affect the Joule heating process? When the neutral density is large enough to increase the Pedersen conductivity to a sufficiently large level, ion energization proportional to the prescribed potential difference occurs. At ionospheric altitudes below ~500 km, it is often assumed that this is the major source of ion heating *[St. Maurice and Schunk, 1999; St. Maurice and Hanson, 1997]*. However, some *in situ* observations indicate that this may not always be the case *[Kivanic and Heelis, 1999]*. Those observations show that large scale electric fields inducing **E×B** drifts of near 1 km/s or more are consistent with Joule heating. However, when the electric field becomes highly structured, the data are more consistent with a scenario of wave heating of the ions. The notion of the dissipation of energy in these highly structured flows is also indicated by the ARCS-4 data set *[Moore et al., 1996]*.

Studies have shown that if a given electric field is sufficiently spatially localized, the possibility of wave heating of the ions exists in conditions where the waves are not collisionally damped. Broadband waves in the ion-cyclotron frequency range can be generated by the shear in the **E×B** rotation *[Ganguli et al., 1988;Koepke et al., 1994; Amatucci et al., 1996]*. Wave heating occurs when the Doppler shifted wave frequency observed in the frame of the **E×B** drifting ions overlaps harmonics of the ion cyclotron frequency*[Ganguli et al., 1985a,b; Walker et al., 1997; Amatucci et al., 1998]*. Structured electric fields, broadband waves, and transverse ion heating are frequently observed in collisionless conditions in the topside auroral F-region *[Andre et al., 1990; Lynch et al., 1996; Kintner et al., 1996]*.

The mechanism by which ion heating occurs (i.e., wave and/or Joule heating) has important geophysical consequences since heavy ion (oxygen) distribution functions measured at higher altitudes often display heating which is argued to have been generated lower in the ionosphere *[Klumpar, 1979]*. The low altitude origin of the ions is particularly evident in the auroral regions where transverse heating and outflow of oxygen ions are routinely observed. Since these ions are most abundant at low altitudes where the neutral density is increasing, the dominant mechanism for ion heating is not always clear.

In a recent paper we have treated the relationship and transition regimes between wave and collisional heating *[Amatucci et al., 1999]*. In particular we have demonstrated in that work that for plasma conditions such that the ion neutral collision frequency is sufficiently small to allow wave growth, energy dissipation which occurs through wave-particle interactions can be the primary channel of heating, even in those cases where both heating mechanisms are possible. However, at higher collision frequencies where these waves are collisionally damped, only the Joule-heating regime is observed. We concentrate in this work on demonstrating this ion heating in the collisional regime for a variety of localized transverse electric field strengths and scale lengths and compare the measured heating to Joule heating as a function of collisionality (i.e., as a function of neutral pressure).

II. Experimental Environment and Measurement Description

The experimental device is the Naval Research Laboratory's Space Physics Simulation Chamber (SPSC) whose available parameter ranges makes it particularly appropriate for studying both wave and collisional heating regimes and the transition between the two. The cylindrical device which is 5 m long and has a diameter of 1.8 m is covered in detail in earlier work *[Walker et al., 1997]*. In addition there are a set of 5 surrounding magnetic field coils arranged in a Helmholtz fashion. We are able to provide a constant axial magnetic field of up to 50 gauss along the length of the chamber. The density of the argon plasma created by collisional ionization is $n \approx 10^9$ cm^{-3} and ambient temperatures of ions and electrons are typically $T_i \approx 0.05$ eV and $T_e \approx 0.2$-0.3 eV. The ion gyrofrequency in a 40 gauss field is $\Omega_i \approx 10^4$ rad s^{-1} and the ion gyroradius is near $\rho_i \approx 3.5$ cm. Ion thermal speed is $v_{ti} \approx 5 \times 10^4$ cm s^{-1} and neutral argon density varies from $N_n \sim 10^{11} - 10^{14}$ cm^{-3}. Langmuir probes are used as diagnostics of electron temperature and density and the ion temperature measurements are taken with the ion energy analyzer which is described below.

There are 3 different types of plasma sources available, two of which are microwave sources *[Walker et al., 1994; Bowles et al., 1996]*; the experimentation described here employed two separate filament sources. Argon gas was used to produce argon plasma via collisional ionization with the electrons produced by these filament sources. The two filament sources are mounted at opposite ends of the device. Neutral pressure is variable during cryopump operation from near 10^{-3} to 10^{-6} Torr depending upon gas flow rate into the chamber. The method used to control neutral pressure in the chamber employs a leak valve which bleeds neutral argon gas into the experimental area. In this fashion, we are able to effectively simulate lower auroral ionospheric altitude pressure ranges. For a 40 gauss magnetic field this corresponds to near four orders of magnitude variation in the ratio of ion-collision frequency to argon ion-cyclotron frequency, i.e., $10^{-2} < \nu_{in}/\Omega_i < 10$. The ion-neutral collision frequency is obtained using the collision cross section found in Phelps, *[1991]*.

An emissive probe, a Langmuir probe and the ion energy analyzer are the primary plasma diagnostic devices. Plasma potential is obtained from the floating potential of a sufficiently heated emissive probe. A spherical Langmuir probe is swept during runs to provide a measurement of plasma density and electron temperature. The Langmuir probe is regularly heated to mitigate the effects of surface contamination. The ion temperature measurements are taken with a perpendicular energy analyzer whose basis of design and operation is to be found elsewhere *[Katsumata and Okazaki, 1967; Amatucci et al., 1998]*. The probe, which is cylindrical, is placed in the plasma perpendicular to the local magnetic field and collects only ions since electrons are excluded from collection due to small gyroradii (the collector plate is recessed several gyroradii from the grid) and the repelling grid potential. By sweeping the collector potential therefore we are able to obtain an IV trace from which ion temperature can be derived using conventional analysis techniques. We show in Figure 1 sample traces taken with this instrument when sampling the ambient plasma. The two traces show the same data taken both on a linear and a natural log scale. The plasma sampled is determined to have an ion

temperature near 0.076 eV based on the slope of the characteristic seen in the trace. In earlier work with this instrument we observed significant heating in the presence of waves driven unstable by rotational shear induced by threshold **E×B** drifts *[Walker et al., 1997]*.

III. Electric field shaping and localization

To create localized electric fields in the chamber we employ a set of concentric, separately biased conducting rings *[Amatucci, et al., 1996]*. We have recently increased the number of concentric rings used in producing the electric field from 11 to a set of 14 and added a central disk electrode in order to give a wider range in electric field spatial variation. Shown in Figure 2 are typical examples of the creation of a localized electric field in the SPSC. Figure 2a shows plasma potential measured by the emissive probe with the rings disconnected, whereas Figures 2b and 2c contrast different cases where the electric field is inward and outward depending upon the potentials applied to the rings. In these examples we show the creation of potential structures which extend over several ion gyroradii (~ 3.5 cm in the present 40 gauss magnetic field).

An example of varying localization with electric field constant

Since we wish to investigate the effects of varying localization and electric field spatial structure on ion heating, it is often desirable to have the ability to isolate the electric field magnitude from spatial variation. While biasing different groups of rings with respect to one another, we are able to produce wider or narrower structuring while maintaining the field constant. This requires different biases which are determined through a simple linear interpolation algorithm which selects constant electric fields for varying potentials applied. An example of the results of this process is shown in Figure 3. We show in Figure 3a a set of plasma potential profiles selected by the algorithm for this scenario. The plots show plasma potential measured by the emissive probe as a function of radial position across the chamber (the probe was separated by about 30 cm axially from the rings). These potential profiles were produced by biasing a group of contiguous inner rings with respect to an outer, also contiguous, group of rings and varying both the number of rings in each and the voltage applied to each. Each curve represents a different number of rings in the inner relative to the outer group, and a different net applied voltage drop. The net voltage drop varies from 55 to 110 volts with the electric field radially outward in all cases. For example, the five profiles selected were chosen such that the applied potentials varied from +40 volts to +90 volts on the inner ring set with a constant -15 volts on the outer group. The inner ring group varied from 8 rings, plus the central disk, to only 2 rings, plus the central disk. Since there are a total of 14 rings in all, this variation range in the number of rings in the inner group corresponds to a variation of 6 to 12 rings in the outer group. It is clear from this figure that in this manner we have been able to vary the spatial extent (radially) of the high potential regions considerably; from the lowest potential profile(55 volts), where it is perhaps 15 cm in width, to the highest (110 volts) where the width is closer to 24 cm. It also appears that the electric field magnitudes used to select these plots are roughly comparable based on a quick visual inspection of the slopes. That this is indeed the case is shown in Figure

3b where we plot the maximum electric field (derived by differentiating the plasma potential profiles of Figure 3a) versus the full-width-at-half-maximum (fwhm) of the non-zero electric field region.

IV. Results and Conclusions

Equilibrium properties of the plasma

The previous experiments which focused on the relative dominance of wave or Joule heating *[Amatucci, et al., 1999]* utilized electric fields which were directed radially inward. The reason for this is that experimentally, electric fields strong enough and localized enough to give rise to velocity-shear-driven ion-cyclotron waves, could be created without generating significant density gradients. For the experiments reported here, which focus on Joule heating, the electric field was directed radially outward. In this case, there is a self-consistent density gradient. The equilibrium formed in the case of the outward-directed electric field is distinctly different from the previously studied inward-directed field case. In this setup, the diamagnetic drift induced by the strong density gradient effectively cancels the oppositely directed **E x B** drift. Thus, no cross-field flow, and hence, no shear exists, removing the possibility of ion heating via shear driven ion-cyclotron waves. Consequently, this is an ideal case for the study of Joule heating. We treat the effect of this electric field direction reversal and concerns related to cylindrical geometry (as opposed to simple first-order slab geometry) in a more complete extended work-in-progress.

Comparison to Joule Heating Rate

As a zero-order estimate to the validity of our results we calculate the Joule heating rate ignoring any effects of curvature associated with **E x B** rotation of the plasma in our calculations. The Joule heating rate, R, is given by $R = \mathbf{J}_P \cdot \mathbf{E}$, where $\mathbf{J}_P$ is the Pedersen current density defined above. In order to calculate this rate, for comparison to the ion temperature rise, it is necessary to calculate the Pedersen conductivity, Σ_p. We might note that even though we expect a small Hall current in this setup, it would not be a contributing factor in the measured Joule heating since $\mathbf{J}_H \cdot \mathbf{E} = 0$, where $\mathbf{J}_H$ is the Hall current density. The heating rate can therefore be approximated by,

$$R = \Sigma_p E^2 \qquad \textbf{(1)}$$

where, Σ_p depends on both plasma and neutral densities and species along with the magnetic field strength and is given by,

$$\Sigma_p = \left(\frac{N_i e^2}{m}\right) \frac{\nu_{in}}{\nu_{in}^2 + \Omega_i^2} \tag{2}$$

where N_i is plasma density, ν_{in} is the ion-neutral collision frequency, E is the applied field and Ω_i is the ion cyclotron frequency. In the calculation of ν_{in}, we use ion thermal velocity in addition to the cross section, σ, for collision between ions and neutrals (in this case $A_r - A_r^+$) or,

$$\nu_{in} = N_n \sigma \delta V \tag{3}$$

where $\sigma(A_r - A_r^+) \sim 1.5 \times 10^{-18}$ m^2 and $\delta V = v_{th} - v_N$ with v_N as neutral velocity and v_{th} as ion thermal speed.

In Figure 4a we show the relationship between chamber pressure and normalized ion-neutral collision frequency expressed by Eqn. (3) for a magnetic field strength of 40 gauss.. Figure 4b is a plot of Σ_p versus chamber pressure as seen in Eqn. (2) and Eqn (3). We notice from Figure 4 that the conductivity peaks at $(\nu_{in}/\Omega_i) \sim 1$ and therefore that one expects a maximum in the Joule heating rate at this point. The results seen in Figures 5a and 5b are a comparison of measured ion temperature and Joule heating as a function of ion-neutral collision frequency for two different magnetic fields. By varying magnetic field strength for a given range of neutral pressure, we can experimentally control the point where Σ_p maximizes, and hence, control the pressure for which maximum ion heating is expected. We examine first Figure 5a for the higher magnetic field strength (B= 40 G) and notice that these plots are consistent with the theoretical predictions of Figure 4, i.e., over the range of collision frequencies tested there is both a peak observed in the Joule heating rate and in the normalized ion temperature near $(\nu_{in}/\Omega_i) \approx 1$. In both cases, there is a maximum measured when $(\nu_{in}/\Omega_i) \approx 1$. The Joule heating rate is calculated by using the actual value of the electric field derived from the experimentally measured radial profiles of the plasma potential. This same behavior is evident in Figure 5b where we plot the same variables for a magnetic field strength of 10 gauss. Since the ion cyclotron frequency is a factor of 4 lower we are only able to extend the ratio as low as about 1.2, i.e., we are limited to about 10^{-5} Torr pressure in the chamber. Nevertheless the same behavior is observed in the region where data is taken. What is worth noting in this figure is that even though there is an increasing ion-neutral collision frequency, the ion temperature decreases as does the Joule heating rate. It is often assumed that increasing ion-neutral collisions lead to an increasing temperature but clearly this does not occur in the data either.

Further support for ion heating in this scenario is suggested by the spatial separation between the electric field region and the heated ion boundaries shown in Figure 6. We plot in Figure 6a the ion gyroradius, ρ_i, versus the distance from the electric field region boundary for seven different cases when heating is first observed. Two of the seven profiles chosen, showing both the electric field region and results of the ion temperature measurement, are plotted in Figures 6b and 6c. In Figure 6a, a straight line with a slope of one is superimposed to suggest the

correspondence between ρ_i and the separation i.e., heating is observed within approximately one gyroradius of the electric field region. Figure 6d shows ρ_i plotted versus T_i for comparison.

Because of the importance associated with uncovering lower altitude ion heating mechanisms we have performed a series of investigations to characterize Joule heating in ionospheric-like (i.e., structured) electric fields. We have investigated the combined effects of localization and electric field strength on ion temperature for two different axial magnetic field regimes. Based on these experimental results and comparisons to calculations of Joule heating rates as described we feel confident that the heating observed is real and is consistent with lower altitude observations of ion heating in highly collisional regimes.

V. Acknowledgments:

We gratefully acknowledge the support of Mr. Dwight Duncan in the experimental effort. In addition, funding for the work was provided by the Office of Naval Research.

VI. References:

Amatucci, W.E., D.N. Walker, and D. Duncan, Wave and Joule heating in a rotating plasma,, *Phys. Plasmas, 6*, 619, 1999

Amatucci, W.E., D.N. Walker, G. Ganguli, J.A. Antoniades, D. Duncan, J. Bowles, V. Gavrishchaka, and M. E. Koepke, Velocity-shear-driven ion-cyclotron waves and associated transverse ion heating, *J. Geophys. Res., 103*, 11711, 1998

Amatucci, W.E., G. Ganguli, D.N. Walker, J.A. Antoniades, D. Duncan, J.H. Bowles, V. Gavrishchaka, and M.E. Koepke, Plasma Response to strongly sheared flow, *Phys. Rev. lett., 77*, 1978, 1996

Andre, M., G.B. Crew, W.K. Peterson, A.M. Persoon, C.J. Pollock, and M.J. Engebretson, Ion heating by broadband low-frequency waves in the Cusp/Cleft, *J. Geophys. Res., 95(A12)*, 20,809, 823, 1990

Bowles, J.H., D. Duncan, D.N. Walker, W.E. Amatucci and J.A. Antoniades, A large volume microwave plasma source, *Rev. Sci. Instr., 67*, 455, 1996

Ganguli, G., Y.C. Lee and P.J. Palmadesso, Electrostatic ion-cyclotron instability caused by a non-uniform electric field perpendicular to the external magnetic field, *Phys. Fluids, 28*, 761-763, 1985a

Ganguli, G., P.J. Palmadesso, and Y.C. Lee, A new mechanism for excitation of electrostatic ion cyclotron waves and associated perpendicular ion heating, *Geophys. Res. Lett., 12*, 643, 1985b

Ganguli, G. and Y. C. Lee, Kinetic theory for electrostatic waves due to transverse velocity shears, *Phys. Fl., 31*, 823, 1988

Katsumata, I. and M. Okazaki, Ion sensitive probe- A new diagnostic method for plasmas in magnetic fields, *Jpn. J. Appl. Phys., 6*, 123, 1967

Kelley, M.C., *The Earth's Ionosphere*, Academic, San Diego, 1989

Kintner, P.M., J. Bonnell, R. Arnoldy, K. Lynch, C. Pollock, and T. Moore, SCIFER - Transverse ion acceleration and plasma waves, *Geophys. Res. Lett., 23(14)*, 1873, 1996

Klumpar, D.M., Transversely accelerated ions: An ionospheric source of hot magnetospheric ions, *J. Geophys, Res., 84*, 4229, 1979

Koepke, M.E., W.E. Amatucci, J.J. Carroll III, and T.E. Sheridan, Experimental verification of the inhomogeneous energy-density driven instability, *Phys. Rev. Lett., 72*, 3355, 1994

Lynch, K., R. Arnoldy, P. Kintner, and J. Bonnell, The AMICIST auroral sounding rocket--A comparison of transverse ion acceleration mechanisms, *Geophys. Res. Lett., 23(23)*, 3293-3296, 1996

Moore, T.E., M.O. Chandler, C.J. Pollock, D.L. Reasoner, R.L. Arnoldy, B. Austin, P.M. Kintner, and J. Bonnell, Plasma heating and flow in an auroral arc, *J. Geophys. Res., 101*, 5279, 1996

Kivanic and Heelis, On relationships between horizontal velocity structure and thermal ion upwellings at high latitudes, *Geophys. Res. Lett., 26*, 1829, 1999

Phelps, A., Cross sections and swarm coefficients for nitrogen ions and neutrals in N_2 and argon ions and neutrals in Ar for energies from 0.1 eV to 10 keV, *J. Phys. Chem. Ref. Data, 20*, 557, 1991

J. St. Maurice and R. Schunk, Ion velocity distributions in the high latitude ionosphere, *Rev. Geophys. Space Science, 17*, 99(1977)

J. St. Maurice and W. Hanson, Ion frictional heating at high latitudes and its possible use for an *insitu* determination of neutral thermospheric winds and temperatures, *J. Geophys. Res., 87*, 7580 (1982)

Walker, D.N., D. Duncan, J.A. Stracka, J.H. Bowles, C.L. Siefring, M.M. Baumback and P. Rodriguez, A tunable microwave source for space plasma simulation experiments, *Rev. Sci. Instr., 65*, 661, 1994

Walker, D.N., W.E. Amatucci, G. Ganguli, J.A. Antoniades, J.H. Bowles and D. Duncan, Perpendicular ion heating by velocity-shear-driven waves, *Geophys. Res. Lett., 1187*, 1997

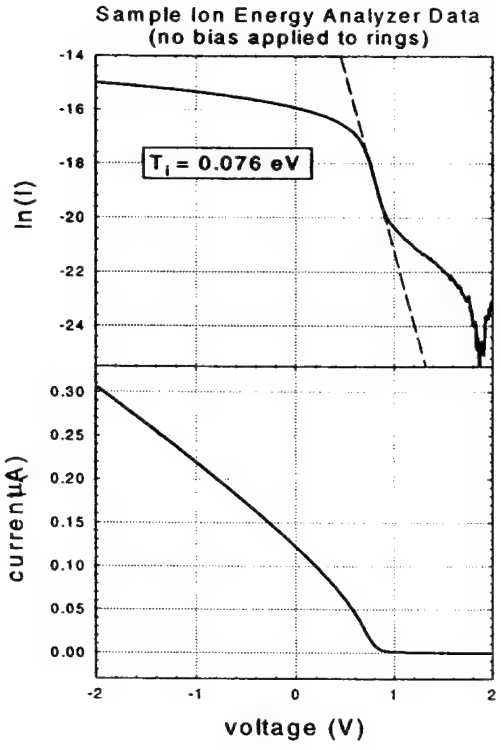
Sample Ion Energy Analyzer Data
(no bias applied to rings)
T_i = 0.076 eV
ln(I)
current(μA)
voltage (V)

Figure (1)

Plasma potential profile
with rings disconnected

(a)

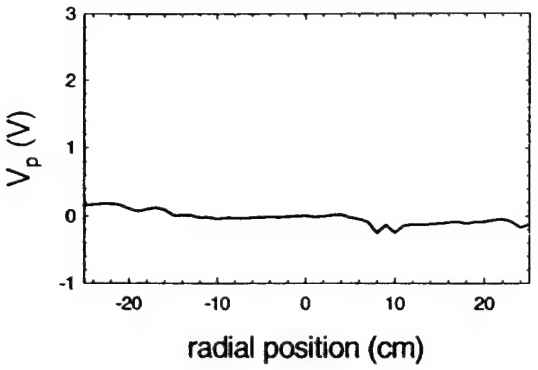

Radially inward-directed
electric field
(disk - ring 5: -100 V;
rings 6 - 14: +5 V)

(b)

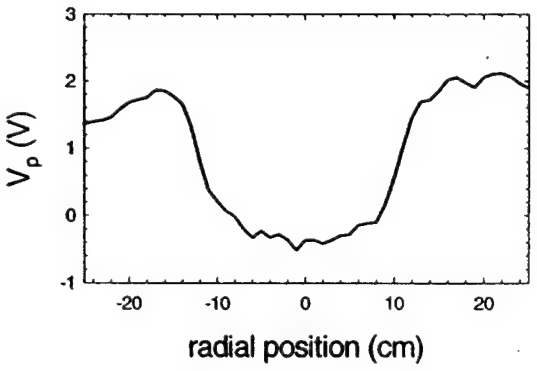

Radially outward-directed
electric field
(disk - ring 6: +50 V;
rings 7 - 14: -40 V)

(c)

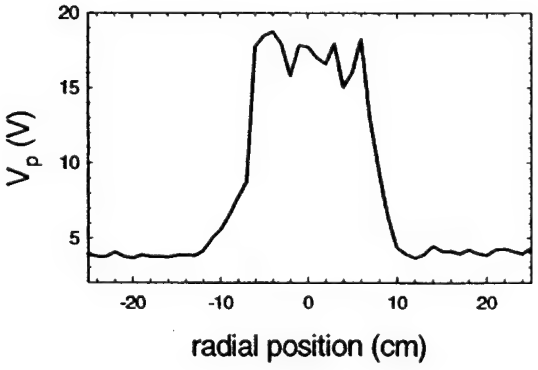

Figure (2)

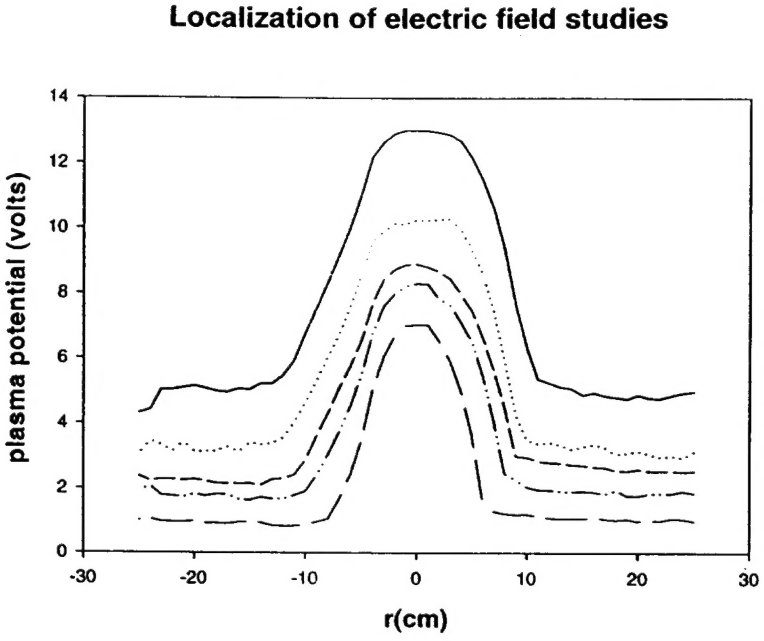
Localization of electric field studies
plasma potential (volts)
14
12
10
8
6
4
2
0
-30
-20
-10
0
10
20
30
r(cm)

(a)

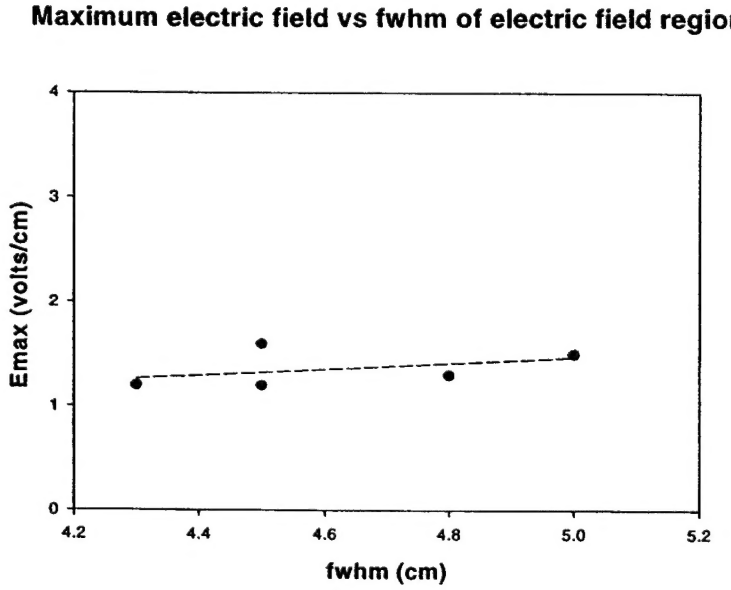
Maximum electric field vs fwhm of electric field region
Emax (volts/cm)
4
3
2
1
0
4.2
4.4
4.6
4.8
5.0
5.2
fwhm (cm)

(b)

Figure (3)

(a)

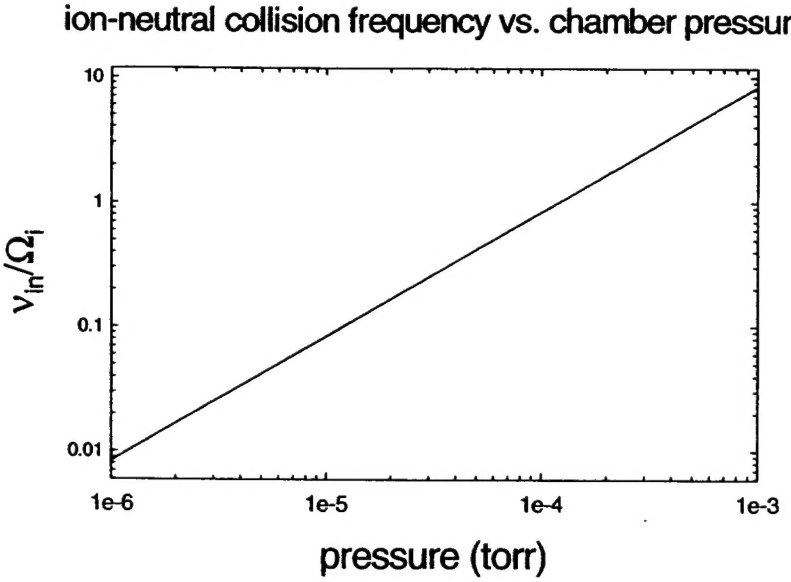
ion-neutral collision frequency vs. chamber pressure
10
1
0.1
0.01
ν_{in}/Ω_i
1e-6
1e-5
1e-4
1e-3
pressure (torr)

(b)

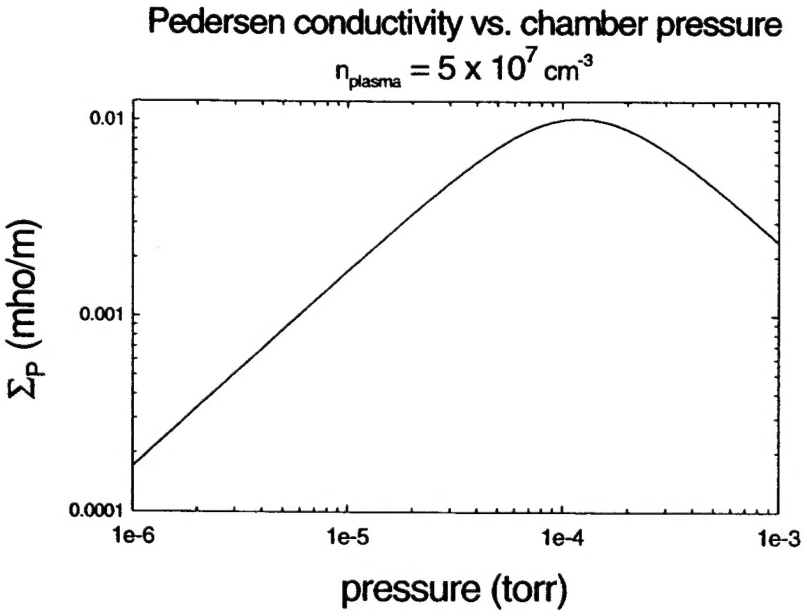
Pedersen conductivity vs. chamber pressure
$n_{plasma} = 5 \times 10^7$ cm^{-3}
0.01
0.001
0.0001
Σ_P (mho/m)
1e-6
1e-5
1e-4
1e-3
pressure (torr)

Figure (4)

B=40 gauss

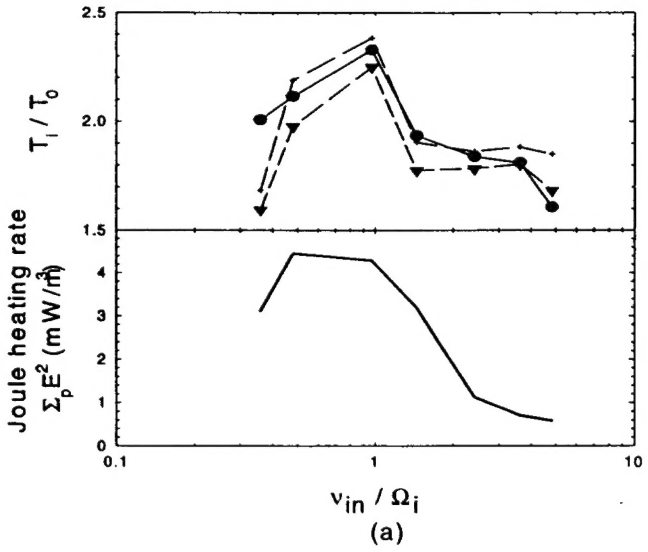

B=10 gauss

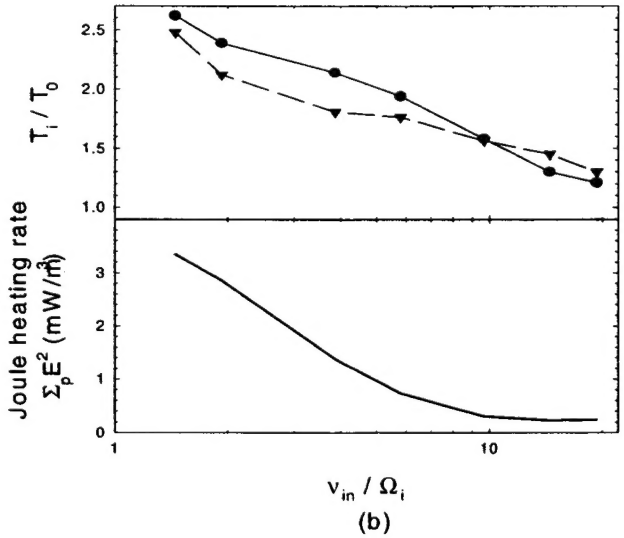

Figure (5)

Spatial Separation Between Electric Field and Heated Ion Boundaries

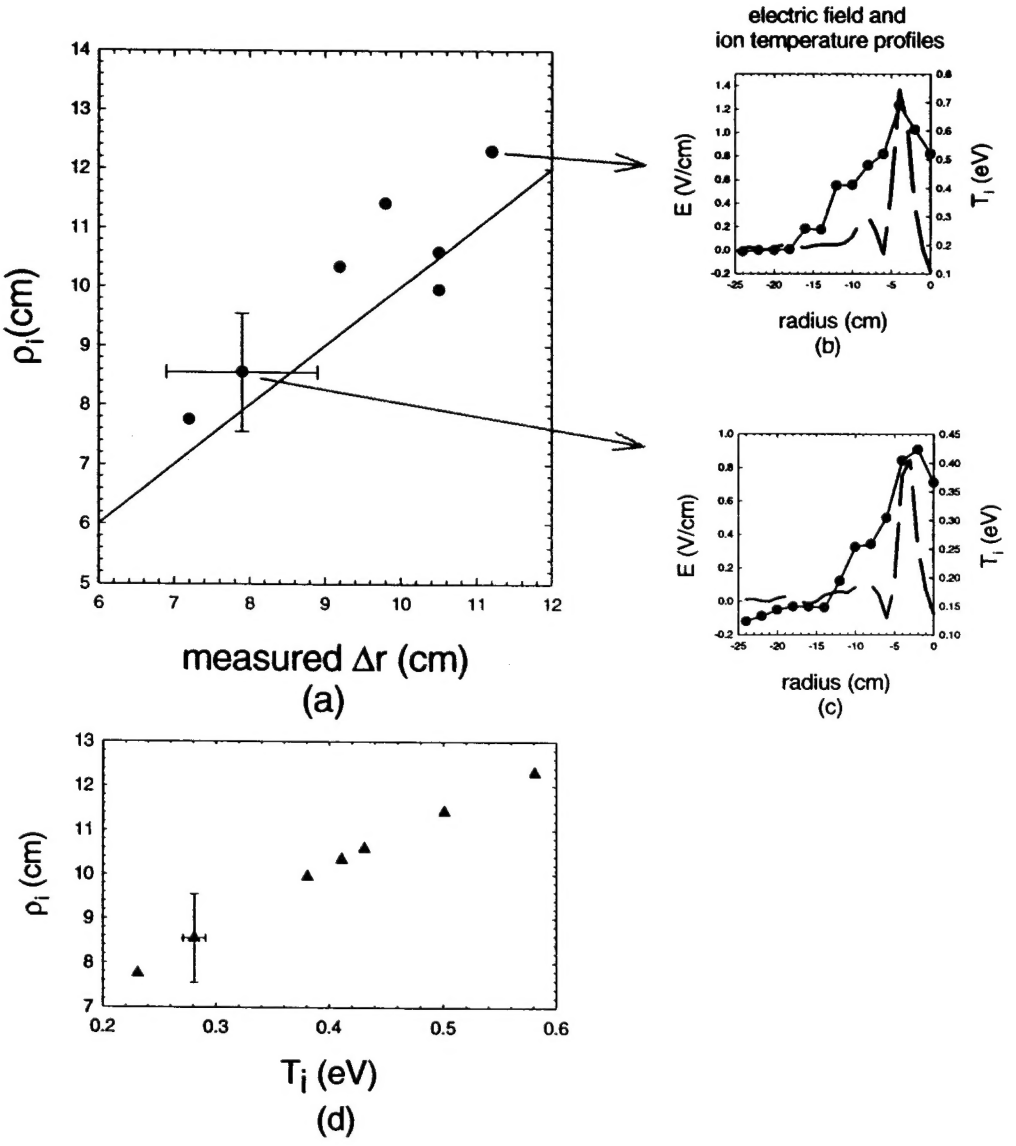

Figure (6)